LEARNING TRANSFERABLE POLICIES BY INFERRING AGENT MORPHOLOGY

Brandon Trabucco CMU btrabucco@cmu.edu
Mariano Phielipp Intel AI mariano.j.phielipp@intel.com
Glen Berseth MILA glen.berseth@mila.quebec

ABSTRACT

The prototypical approach to reinforcement learning involves training policies tailored to a particular agent from scratch for every new morphology. Recent work aims to eliminate the re-training of policies by investigating whether a morphology-agnostic policy, trained on a diverse set of agents with similar task objectives, can be transferred to new agents with unseen morphologies without re-training. This is a challenging problem that required previous approaches to use hand-designed descriptions of the new agent's morphology. Instead of hand-designing this description, we propose a data-driven method that learns a representation of morphology directly from the reinforcement learning objective. Ours is the first reinforcement learning algorithm that can train a policy to generalize to new agent morphologies without requiring a description of the agent's morphology in advance. We evaluate our approach on a standard benchmark for agent-agnostic control, and improve over the state of the art in zero-shot generalization. Importantly, our method attains good performance *without* an explicit description of morphology.

1 INTRODUCTION

Agent-agnostic reinforcement learning is an emerging research challenge that involves training policies that are transferable to new agents with different morphology. Rather than training policies from scratch for every new agent, a pretrained agent-agnostic policy can provide an effective solution with potentially no additional training. In the current deep learning epoch, foundation models (Bommasani et al., 2021, p. 3) demonstrate the promising applications of large-scale transfer learning in other domains. Models like BERT Devlin et al. (2019), GPT-3 Brown et al. (2020), and CLIP Radford et al. (2021) reduce the computational barrier-to-entry often required to obtain high-performance models in downstream applications. Agent-agnostic reinforcement learning as a framework has the potential to enable a similar class of foundation models for control if appropriately scaled. However, being able to scale agent-agnostic reinforcement learning requires an effective neural architecture and a flexible representation for tasks. In agent-agnostic reinforcement learning, tasks are defined by the morphology of the agent Huang et al. (2020), and effectively representing morphology is an open research question. The morphology representation is crucial in agent-agnostic reinforcement learning and directly influences how well the agent generalizes to new tasks. In this work, we investigate how an effective representation of morphology can be learned, rather than manually designed, as in prior work.

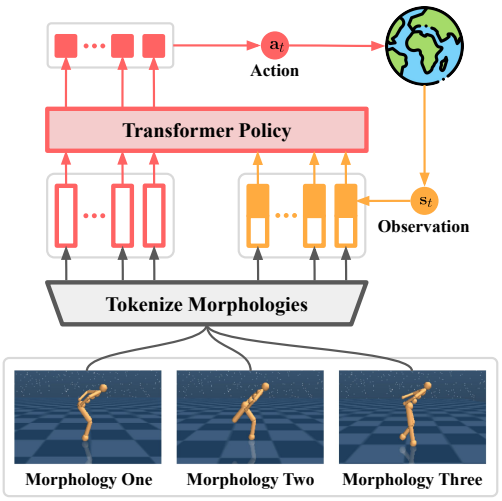

Figure 1: Overview of the architecture of our policy. The agent's morphology is represented by a sequence of tokens, and is processed by a sequence-to-sequence Transformer policy.

Existing works have tackled this question by assuming the agent obeys strict design criteria. First, the agent must have limbs. Second, each limb must have similar propioception Wang et al. (2018);

Table 1: Comparison of assumptions seen in existing literature. Our method is more flexible than prior work, requiring neither graph structure, nor explicitly aligning the agent's sensors and actuators to its limbs in order to generalize effectively. Our approach requires less information about the agent's morphology than prior work, and performs 16% better in zero-shot generalization to new morphologies than existing methods with stronger assumptions, which is discussed in Section 6.

Method \ Assumptions	**Graph Structure**	**Alignment**
Graph Networks Sanchez-Gonzalez et al. (2018)	✗	✗
NerveNet Wang et al. (2018)	✗	✗
Shared Modular Policies (SMP) Huang et al. (2020)	✗	✗
Amorpheus Kurin et al. (2021)		✗
Ours		

Huang et al. (2020); Kurin et al. (2021). These assumptions restrict agent-agnostic reinforcement learning to rigid-body agents in a MuJoCo-like Todorov et al. (2012) simulator that exposes per-limb observations. Deviating from prior work, we investigate an architecture that does not require these strict assumptions , instead learning a representation of morphology with reinforcement learning. Our approach performs 16% better (see Section 6) than existing methods in zero-shot generalization, and requires *less* information about the morphology of the agent being controlled than prior art.

In this paper, we make the following contributions. First, we frame learning morphology as a sequence modelling problem, and represent an agent's morphology as a sequence of tokens, with corresponding learnt embeddings. In this fashion, an agent's morphology is differentiable, and is optimized from the reinforcement learning objective. Second, we propose an agent-agnostic neural network architecture that generalizes effectively and does not assume the agent has limbs, nor has per-limb observations. Third, our approach generalizes up to 32% better than existing work on large tasks in a standard benchmark, and displays an emergent robustness to broken sensors.

2 Related Works

Generalization in reinforcement learning has a rich history, with early works demonstrating generalization to new tasks in robotics Sutton et al. (2011), and in video games Schaul et al. (2015); Parisotto et al. (2016). Tasks were often defined via goal states Sutton et al. (2011), with a reinforcement learning objective defined as minimizing the distance to the goal throughout an episode Andrychowicz et al. (2017); Nasiriany et al. (2019). These goal-based methods can be improved combining them with language Jiang et al. (2019), and learnt latent spaces Eysenbach et al. (2019); Rakelly et al. (2019). As the field matures, researchers are beginning to investigate larger-scale multi-task reinforcement learning (MTRL) Vithayathil Varghese & Mahmoud (2020), including generalization across all of Atari Hafner et al. (2020), and generalization to new agents with different dynamics or morphology. The latter is an emerging topic called agent-agnostic reinforcement learning Devin et al. (2017); III et al. (2020); Huang et al. (2020). This setting is challenging because different agents typically have incompatible (different cardinality) observations and actions, which precludes conventional deep reinforcement learning approaches.

Conventional deep reinforcement learning approaches expect fixed-size observations and actions, and devising effective alternatives is an open research challenge. Existing work has shown modularization can both improve multi-task generalization Chang et al. (2021); Goyal et al. (2021), and allow processing of different-cardinality observations and actions Huang et al. (2020). Many such approaches utilize Graph Neural Networks Gori et al. (2005); Scarselli et al. (2005), conditioning the policy on a graph representation of the agent's morphology. Graph-based approaches have demonstrated the ability to generalize to novel agent morphology Huang et al. (2020), and learn complex gaits Wang et al. (2018); Sanchez-Gonzalez et al. (2018). However, recent work has shown that generalize can be further improved using Transformers Kurin et al. (2021), due to their success in modelling dynamic structure via the attention mechanism Tenney et al. (2019); Vig & Belinkov (2019). Agent-agnostic reinforcement learning methods, including those with Transformers, currently rely on a manually-designed representation of morphology (see Section 3). Our approach differs

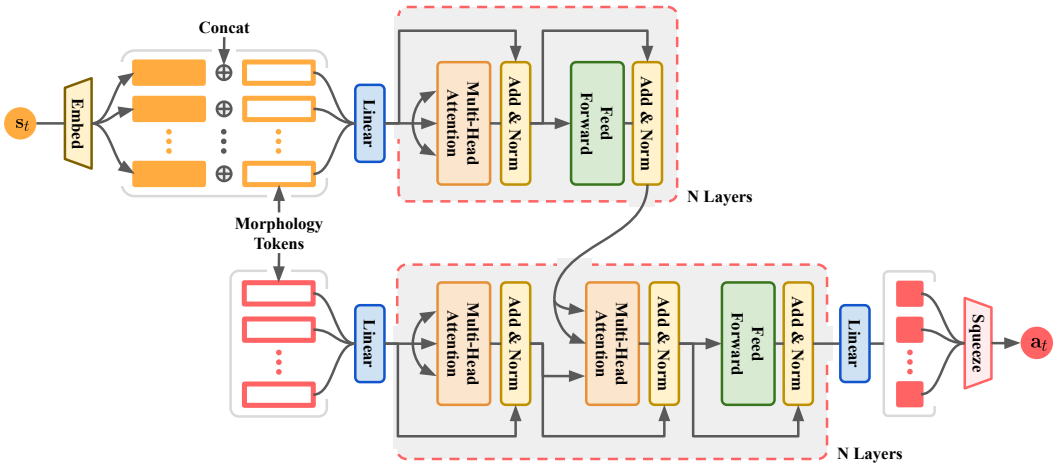

Figure 2: Visualization of the architecture of our policy. Our policy is a sequence-to-sequence deep neural network, consisting of a Transformer Vaswani et al. (2017) encoder that processes the current state $\mathbf{s}_t$ and a sequence of observation tokens (see Section 4), with a Transformer decoder that processes a sequence of action tokens, given the encoder hidden state. Our policy is invariant to the dimensionality of observations and actions, and does not assume the agent has limbs.

from prior work by instead learning a representation of morphology with reinforcement learning that produces better generalization than a manually-designed representation.

3 How Do We Represent Morphology?

The goal of this section is to outline what information is needed to define a *morphology*. This terminology is used, for example, to denote an interpretation of the physical rigid-body of a MuJoCo-like Todorov et al. (2012) agent as a graph, where nodes correspond to rigid limbs, and edges indicate two limbs are connected by a joint. This terminology is based on classical work on kinematic chains (Denavit & Hartenberg, 1955). In this section, we will explore how morphology is used in existing work, and will discuss its benefits and limitations. Towards this goal, we first introduce the reader to notation that will be referred to throughout our paper.

Defining Morphology As A Graph. The *morphology* of a decision-making agent is often represented as a graph. Consider the agent-conditioned undirected graph $\mathcal{G}_n = (V_n, E_n)$ whose vertices V_n each represent a limb the agent has, and whose set of edges E_n contains all pairs of limbs that are connected by a joint. For the typical MuJoCo-like Todorov et al. (2012) agent from prior work, the topology of this graph closely resembles the topology of the agent's body.

$$V_n = \{1 \dots N_L(n)\} \tag{1}$$

$$E_n = \{(i, j) : i \text{ and } j \text{ are connected limbs}\} \tag{2}$$

Defining morphology in terms of $\mathcal{G}_n$ intuitively mirrors how the agent is physically connected; however, it is not a complete description of the agent. Notice the number of limbs $N_L(n)$ is not necessarily equal to the dimensionality of the action space $N_A(n)$. In order to generate an action using a morphology defined in terms of the agent's limbs, one needs a mapping from limbs to actions.

$$F_n^{\text{act}} : \{1 \dots N_L(n)\} \longrightarrow \text{powerset}(\{1 \dots N_A(n)\}) \tag{3}$$

This mapping permits each limb to generate a different number of control signals, mentioned by Huang et al. (2020, p. 6) , at the expense of the researcher designing this mapping ahead of time. In prior works, a shared neural module generates control signals for each limb Sanchez-Gonzalez et al. (2018); Wang et al. (2018); Huang et al. (2020), even when E_n is withheld, as is the case in newer works such as Kurin et al. (2021, p. 4). That module requires a limb-specific input, which we call the local observation, defined by the additional mapping F_n^{obs} from limbs to observations.

$$F_n^{\text{obs}} : \{1 \dots N_L(n)\} \longrightarrow \text{powerset}(\{1 \dots N_S(n)\}) \tag{4}$$

Consequences Of The Graph Definition. One appealing quality of this definition of morphology is that it has an intuitive physical interpretation. Given only the morphology, one can invert the definition to recover the agent's physical design, including the arrangement of its sensors. This appealing quality comes at the expense of strict design criteria, however. In this section, we will discuss several consequences of the graph definition of morphology. (1) First, this definition assumes the agent's physical design can be expressed as a graph, which restricts methods to MuJoCo-like Todorov et al. (2012) agents with rigid limbs, which is not true, for example, for a car with flexible rubber tires. We refer to this as the **graph structure assumption**, and categorize prior work using this assumption in Table 1. The community is interested in the eventual application of agent-agnostic reinforcement learning in real-world robotic systems. We speculate that a graph inductive bias may be insufficient to represent the complex physique of certain agents. (2) Another common assumption is that sensors and actuators are categorizable according to a particular limb. Methods with this **alignment assumption** in Table 1 only maintain agnosticism to limbs, and not to individual sensors and actuators Huang et al. (2020); Kurin et al. (2021). Some interesting reinforcement learning problems violate this property by not having per-limb sensors, or well-defined limbs. Tackling these problems may require more flexible methods that do not require aligning sensors to limbs.

4 Morphology As Sequence Modelling

Defining morphology in terms of limbs, which we discussed in Section 3, often requires making three unrealistic assumptions about the agent (see Table 1). In this section, we will present an alternate representation of morphology for general decision-making agents that *outperforms* existing methods while being applicable to a larger space of agent types. We approach this problem by considering two algorithmic desiderata: for a given agent n, (1) our method should be invariant to the dimensionality of the agent's observations and actions, and (2) our method should only be given *minimal* information about the agent's morphology. Our first insight is to interpret the reinforcement learning policy that accepts a state vector and outputs an action vector as sequence-to-sequence mappings, where the source sequence has $N_S(n)$ elements, and the target sequence has $N_A(n)$ elements. This interpretation bypasses all dependence on limbs by defining morphology in terms of which sensors and actuators comprise the agent. Inspired by the success of word embeddings Mikolov et al. (2013) in language modelling, and their role in transferable models like BERT Devlin et al. (2019), we propose to encode sensors and actuators as a sequence of tokens, and represent them with learnt embeddings. We learn embeddings that represent observation and action tokens.

$$H_n^{\text{obs}} \in \mathbb{R}^{N_S(n) \times D},\ H_n^{\text{act}} \in \mathbb{R}^{N_A(n) \times D} \tag{5}$$

Each token encodes the identity of a single sensor or actuator. Embeddings representing these tokens are learned jointly with our policy directly from the reinforcement learning objective. Our policy is a sequence-to-sequence deep neural network that maps from a source sequence with $N_S(n)$ elements to a target sequence with $N_A(n)$ elements. We implement our policy as a variant of the Transformer Vaswani et al. (2017) due to its success in multiple reinforcement learning settings Kurin et al. (2021); Janner et al. (2021); Chen et al. (2021). In the following section, we describe our architecture (shown in Figure 2), and modifications that make it suitable for agent-agnostic reinforcement learning.

Morphology Tokens. Before detailing our policy architecture, we will explore how observation embeddings H_n^{obs} and action embeddings H_n^{act} can be obtained. In the previous section, we described a corresponding set of observation tokens I_n^{obs} and action tokens I_n^{act} that are represented by these embeddings. These tokens are represented by integers that uniquely identify the agent's morphology.

$$I_n^{\text{obs}} \in \mathbb{N}^{N_S(n)},\ I_n^{\text{act}} \in \mathbb{N}^{N_A(n)} \tag{6}$$

We refer to the pair $(I_n^{\text{obs}}, I_n^{\text{act}})$ as *morphology tokens*. These tokens index into a pair of morphology embeddings W_e^{obs}, and W_e^{act} that are weight matrices with D columns. Each weight matrix learns to embed each sensor and actuator for each morphology in the set of N agents. In practice, not every row will be used because different agent morphologies share a portion of the same tokens.

$$W_e^{\text{obs}} \in \mathbb{R}^{\left(\prod_{i=1}^{N} N_S(i)\right) \times D} \tag{7}$$

$$W_e^{\text{act}} \in \mathbb{R}^{\left(\prod_{i=1}^{N} N_A(i)\right) \times D} \tag{8}$$

Given the pair of morphology tokens and morphology embeddings, we use an embedding lookup operation in order to obtain the pair of observation and action token embeddings H_n^{obs} and H_n^{act} for each morphology. Recall from Equation 5 these have a fixed number of columns, and a variable number of rows, which depends on the dimensionality of the agent's observations and actions.

$$H_n^{\text{obs}} = \text{embedding\_lookup}\left(I_n^{\text{obs}},\ W_e^{\text{obs}} \right) \tag{9}$$

$$H_n^{\text{act}} = \text{embedding\_lookup}\left(I_n^{\text{act}},\ W_e^{\text{act}} \right) \tag{10}$$

These observation and action token embeddings are shown in Figure 2 as a sequence of outlined rectangles on the left of the diagram. Each colored rectangle in each sequence represents a token embedding vector with cardinality D. Outlined yellow rectangles represent observation tokens, and outlined red rectangles represent action tokens. While this representation of morphology does not require the agent to have limbs, it requires instead a pair of morphology tokens that identify the agent's sensors and actuators. Since this representation is continuous and differentiability, one promising option to avoid manual annotation is to infer H_n^{obs} and H_n^{act} using an encoder.

Embedding The Current Observation. How can we condition our policy, which is a sequence to sequence model, on the current state? We propose to view the current state as a sequence with $N_S(n)$ elements, embedding each element to a M-vector, and concatenate it with the matrix of observation token embeddings H_n^{obs} column-wise. We empirically find that passing the state through a sinusoidal embedding function before concatenation helps the model to perform well, which may be interpreted as increasing the expressivity of the model class Li & Pathak (2021). Our embedding function passes the state through a series of M sinusoidal functions with geometrically increasing frequencies $k_1, k_2, \ldots k_{\lfloor M/2 \rfloor}$ from $1/10$ to 1000. In Figure 2, we represent this operation with the yellow trapezoid labelled embed on the left, and denote the subsequent concatenation of the embedded state with H_n^{obs} via the plus symbol.

$$X = \Big[\ H_n^{\text{obs}};\ \underbrace{\cos\left(k_1 \mathbf{s}_t\right);\ \sin\left(k_1 \mathbf{s}_t\right);\ \ldots}_{M \text{ columns}}\ \Big] \tag{11}$$

Before processing X and H_n^{act} with our transformer, we apply a linear transformation that maps them to the cardinality of the Transformer hidden state. We learn two linear transformations W_p^{obs} and W_p^{act} for observation and action embeddings respectively, projecting to d_{model} components.

$$W_p^{\text{obs}} \in \mathbb{R}^{(D+M)\times d_{\text{model}}},\ W_p^{\text{act}} \in \mathbb{R}^{D \times d_{\text{model}}} \tag{12}$$

After projection, we process these embeddings with a Transformer encoder-decoder model, following the architecture presented by Vaswani et al. (2017, p. 3). We drop autoregressive masking, which is unnecessary in our setting. Details about the hyperparameters used with our model can be found in Appendix B. The output of our Transformer is a sequence of $N_A(n)$ hidden states with d_{model} components. To generate actions, we learn a projection W_p^{out} from d_{model}-vectors to scalars. Our model outputs a vector y_t with $N_A(n)$ components, representing pre-activation actions.

$$W_p^{\text{out}} \in \mathbb{R}^{d_{\text{model}}} \tag{13}$$

$$\mathbf{y}_t = \text{Transformer}\big(XW_p^{\text{obs}},\ H_n^{\text{act}}\ W_p^{\text{act}} \big) W_p^{\text{out}} \tag{14}$$

With a final hyperbolic tangent activation, we generate the mean action $\mathbf{a}_t = \tanh(\mathbf{y}_t)$ for the current timestep. This conversion from Transformer outputs to actions is shown in Figure 2 by the Linear and Squeeze boxes on the right. By framing learning morphology as sequence modelling, our model is applicable to a larger space of agent types, given appropriate morphology tokens and sufficient training. Furthermore, our model does not assume the agent conforms to strict design criteria seen in prior work and detailed in Section 3. In the remaining sections, we will benchmark our model on a standard set of agent-agnostic reinforcement learning tasks, and visualize what our model learns.

5 Training Performance

We have constructed a method that is agnostic the morphology of an agent. This model is trained across a collection of different agents to develop generalization skills to new morphologies. To understand how well our method succeeds we evaluate three aspects of the model. First, how quickly

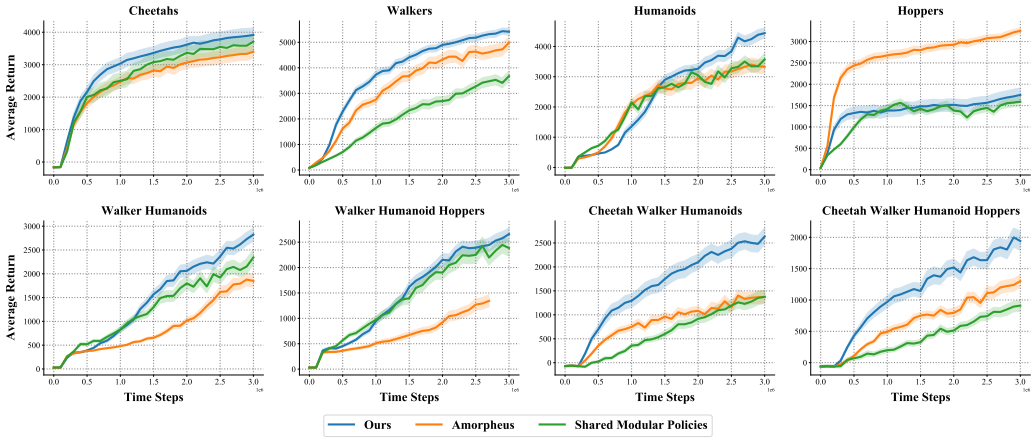

Figure 3: Average return of our method versus Amorpheus (Kurin et al., 2021) and Shared Modular Policies (Huang et al., 2020) across 4 random seeds. Performance on the y-axis is the average return with one episode per training morphology per seed. Dark colored lines indicate the average training performance, and a 95% confidence interval is shown with shading around each line. The x-axis indicates the total steps across all training morphologies. Our method frequently reaches and exceeds the performance of baselines, improving by 85% and 53% on the Cheetah-Walker-Humanoids and Cheetah-Walker-Humanoid-Hoppers tasks respectively, the two hardest tasks.

can we train the morphology agnostic policy. We should receive gains in sample efficiency as the model learns how to share experience across morphologies. Second, how well does the method generalize to novel morphologies not seen during the training process. Last, how robust is our method to sensor issues. To answer these question, we leverage a benchmark for agent-agnostic reinforcement learning developed by Huang et al. (2020, p. 1). This benchmark contains a set of eight reinforcement learning tasks, where the goal is to maximize the average return over a set of N agents with different morphologies. The agents present in this benchmark and inspired by and derived from standard OpenAI Gym tasks: HalfCheetah-v2, Walker2d-2, Hopper-v2, and Humanoid-v2 Brockman et al. (2016). For the Cheetahs, Walkers, Humanoids, and Hoppers tasks, there are a total of 15, 6, 8, and 3 different morphologies used in prior work Kurin et al. (2021); Huang et al. (2020). The benchmark consists of four tasks containing morphologies of a single *kind* of agent (see Cheetahs, Walkers, Humanoids, and Hoppers in Figure 3), and four tasks that mix together multiple kinds of agents (see Walker-Humanoids, Walker-Humanoid-Hoppers, Cheetah-Walker-Humanoids, and Cheetah-Walker-Humanoid-Hoppers in Figure 3). Solving the latter mixed tasks requires the policy to acquire gaits that generalize to multiple kinds of agents. The two hardest tasks in the benchmark are Cheetah-Walker-Humanoids, and Cheetah-Walker-Humanoid-Hoppers, which involve controlling 29 and 32 different agent morphologies respectively.

Our method excels at training on many morphologies at once, and sees greater improvements as the amount of morphologies increases. Shown in Figure 3, on all tasks but Hoppers, our policy meets and exceeds the performance of Amorpheus Kurin et al. (2021) and Shared Modular Policies Huang et al. (2020). Furthermore, on the hardest tasks, Cheetah-Walker-Humanoids, and Cheetah-Walker-Humanoid-Hoppers, we see an improvement of 85% and 53% respectively. This improvement suggests that our method can scale more effectively than prior work, as it trains across up to 32 different morphologies, and maintains a strong performance gain. Our methods performs consistently well across all tasks except Hoppers. The Hoppers task has only three morphologies, the fewest in the benchmark, and we suspect this relates to our diminished performance.

6 Zero-Shot Generalization

In the previous section, we evaluated the training performance of our model, and demonstrated a significant improvement when controlling many morphologies. Now we ask, how well does our model generalize to new morphologies it was not trained on? To answer this question, we follow Kurin et al.

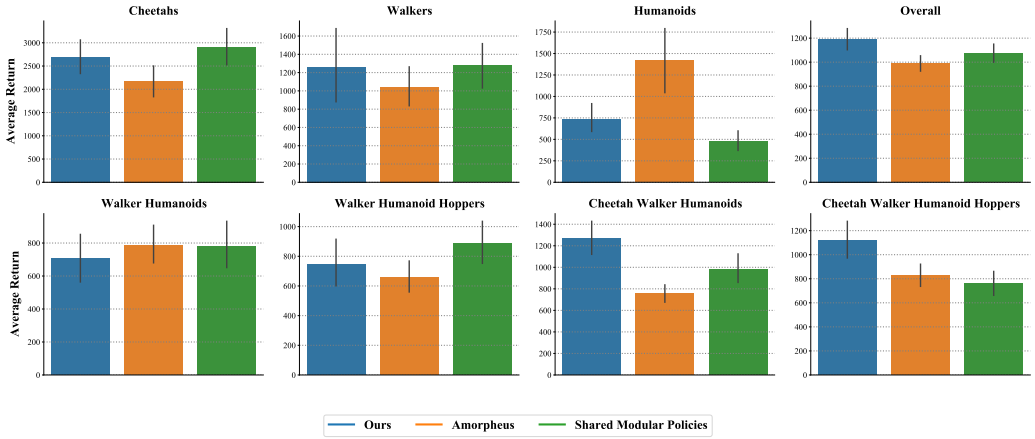

Figure 4: Average return of our method versus Amorpheus (Kurin et al., 2021) and Shared Modular Policies (Huang et al., 2020) for held-out morphologies with 4 random seeds. Performance on the y-axis is the average return with ten episodes per held-out morphology per seed. Colored bars represent average performance evaluated at 2.5 million environment steps, and a 95% confidence interval is shown with error bars. Overall performance is an aggregation of all episodes from each method. Our model improves by 16% overall, and by 28% and 32% on the Cheetah-Walker-Humanoids and Cheetah-Walker-Humanoid-Hoppers tasks respectively, the two hardest tasks.

(2021) and hold out 3 Cheetahs, 2 Walkers, and 2 Humanoids respectively. See Appendix C for which specific morphologies are used for testing. We then evaluate the policies learned by our method, Amorpheus, and Shared Modular policies at 2.5 million environment steps on each morphology that are held out. For tasks that involve multiple kinds of agents, we evaluate using all held out morphologies for each kind. We report the average return for each method over 4 random seeds, and ten episodes per seed, with a 95% confidence interval in Figure 4.

Despite not explicitly conditioning on morphology via graph structure or sensor-to-limb alignment, our method improves by 16% in overall zero-shot generalization. On tasks with fewer morphologies, our methods performs on par with existing methods, with an exception on the Humanoids tasks. We obtain an improvement of 28% on Cheetah-Walker-Humanoids, and 32% on Cheetah-Walker-Humanoid-Hoppers, the two hardest tasks in the benchmark. The disparity between training and testing performance on certain tasks (such as the Humanoids task) suggests observing many morphologies during training is key to regularization that enables our model to generalize effectively.

7 Visualizing Robustness

In the two previous experiments, we evaluated the training performance and zero-shot generalization ability of our model, and displayed compelling gains. One remaining question, however, is how resilient our model is to *minor* changes in the agent's morphology, caused by one or more sensors breaking. We investigate this question by designing an experiment where a fraction of the agent's sensors are replaced with noise sampled from the standard normal distribution. The goal of this experiment is to evaluate the robustness of our model, measured by average return, as a function of how many of the agent's sensor readings (state features) are replaced with random noise. Our methodology for selecting the order to corrupt sensors is described in Appendix D. An evaluation of the robustness of our method compared to prior works is presented in Figure 5, where the average return for each method given a certain fraction of corrupted sensors is calculated from one episode per morphology per task using deterministic actions, with 4 random seeds per method on each task. Training average return is plotted on the y-axis, with a 95% confidence interval.

This experiment demonstrates that our policy architecture is more robust to broken sensors than prior works. Our policy achieves a higher area under the curve on all eight tasks. Though our method initially performs worse than Amorpheus (illustrated in Figure 3) on the Hoppers task, broken sensors quickly cripple existing methods. One promising hypothesis for this improved robustness

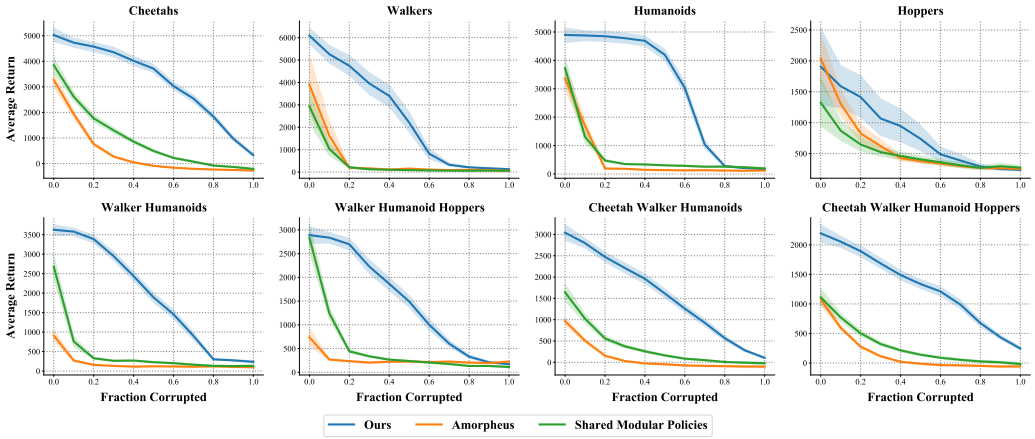

Figure 5: Average return of our method versus Amorpheus Kurin et al. (2021) and Shared Modular Policies Huang et al. (2020) as a function of how many sensors are corrupted by random noise. Performance on the y-axis is the average return of 4 random seeds with one episode per training morphology for each seed, evaluated at 2.5 million steps. Dark colored lines indicate the average performance for each method given a fraction of sensors that are corrupted by noise sampled from a standard normal distribution, and a 95% confidence interval is shown with shading around each line. The x-axis indicates the fraction sensors in the agent's observation space are corrupted with noise. Our method consistently improves robustness, illustrated by a greater area under the curve.

is that our model is actively ignoring certain sensors. To evaluate this hypothesis, we visualize the attention weights throughout an episode in the final cross attention mechanism in our model (that is, actuator-to-sensor attention) in Figure 6. For each cell in the visualization, we take the maximum attention weight over an entire episode (rows no longer sum to one) for one trial on the Humanoids task and Humanoid 2d Full morphology. This visualization shows that our model learns sparse attention weights that ignore the majority of sensors, shown by the majority of dark cells in the visualization. This quality in the attention weights suggests our model improves robustness by sparsely attending to sensors.

8 Conclusion

We have presented a method for learning transferable policies between agents of different morphology, by inferring the agent's morphology via a learned embedding. Our approach is more scalable than existing methods, and is able to learn composable polices for up to 32 different morphologies at once while maintaining a performance lead of 82% in training, and 32% in zero-shot generalization on our benchmarking task with the most morphologies. Our method operates by framing learning morphology as a sequence modelling problem, and learns a Transformer-based policy that is invariant to the dimensionality of the agent's observations and actions. In addition to improving performance, we demonstrate that our policy is more resilient to broken sensors than existing methods. Importantly, our method attains these improvements while also relaxing the amount of information required about the agent's design compared to prior work. Our method does not require the agent to have limbs, graph structure, or aligned sensors and actuators. By relaxing these assumptions, our approach improves the applicability of agent-agnostic learning in a more general reinforcement learning context.

Our research is a step towards broadly applicable agent-agnostic reinforcement learning methods, and there are several opportunities to expand our work. Firstly, we observed in Section 6 that our methods benefits from observing many morphologies during training. Further scaling of our method to agent-agnostic reinforcement learning tasks with significantly more morphologies may further improve zero-shot generalization. Secondly, we evaluated our method on MuJoCo-like agents with rigid limbs in this work. Applying our method to reinforcement learning tasks *without* an underlying graph structure or aligned sensors and limbs (such as Atari) poses an interesting challenge. Finally, our method requires morphology tokens (see Section 3) for each agent. Inferring these tokens from

trajectories the agent has collected may enable our method to generalize out-of-the-box without requiring any manual annotation of the task.

REFERENCES

Marcin Andrychowicz, Dwight Crow, Alex Ray, Jonas Schneider, Rachel Fong, Peter Welinder, Bob McGrew, Josh Tobin, Pieter Abbeel, and Wojciech Zaremba. Hindsight experience replay. In Isabelle Guyon, Ulrike von Luxburg, Samy Bengio, Hanna M. Wallach, Rob Fergus, S. V. N. Vishwanathan, and Roman Garnett (eds.), *Advances in Neural Information Processing Systems 30: Annual Conference on Neural Information Processing Systems 2017, December 4-9, 2017, Long Beach, CA, USA*, pp. 5048–5058, 2017. URL https://proceedings.neurips.cc/paper/2017/hash/453fadbd8a1a3af50a9df4df899537b5-Abstract.html.

Rishi Bommasani, Drew A. Hudson, Ehsan Adeli, Russ Altman, Simran Arora, Sydney von Arx, Michael S. Bernstein, Jeannette Bohg, Antoine Bosselut, Emma Brunskill, Erik Brynjolfsson, Shyamal Buch, Dallas Card, Rodrigo Castellon, Niladri S. Chatterji, Annie S. Chen, Kathleen Creel, Jared Quincy Davis, Dorottya Demszky, Chris Donahue, Moussa Doumbouya, Esin Durmus, Stefano Ermon, John Etchemendy, Kawin Ethayarajh, Li Fei-Fei, Chelsea Finn, Trevor Gale, Lauren Gillespie, Karan Goel, Noah D. Goodman, Shelby Grossman, Neel Guha, Tatsunori Hashimoto, Peter Henderson, John Hewitt, Daniel E. Ho, Jenny Hong, Kyle Hsu, Jing Huang, Thomas Icard, Saahil Jain, Dan Jurafsky, Pratyusha Kalluri, Siddharth Karamcheti, Geoff Keeling, Fereshte Khani, Omar Khattab, Pang Wei Koh, Mark S. Krass, Ranjay Krishna, Rohith Kuditipudi, and et al. On the opportunities and risks of foundation models. *CoRR*, abs/2108.07258, 2021. URL https://arxiv.org/abs/2108.07258.

Greg Brockman, Vicki Cheung, Ludwig Pettersson, Jonas Schneider, John Schulman, Jie Tang, and Wojciech Zaremba. Openai gym. *CoRR*, abs/1606.01540, 2016. URL http://arxiv.org/abs/1606.01540.

Tom B. Brown, Benjamin Mann, Nick Ryder, Melanie Subbiah, Jared Kaplan, Prafulla Dhariwal, Arvind Neelakantan, Pranav Shyam, Girish Sastry, Amanda Askell, Sandhini Agarwal, Ariel Herbert-Voss, Gretchen Krueger, Tom Henighan, Rewon Child, Aditya Ramesh, Daniel M. Ziegler, Jeffrey Wu, Clemens Winter, Christopher Hesse, Mark Chen, Eric Sigler, Mateusz Litwin, Scott Gray, Benjamin Chess, Jack Clark, Christopher Berner, Sam McCandlish, Alec Radford, Ilya Sutskever, and Dario Amodei. Language models are few-shot learners. In Hugo Larochelle, Marc'Aurelio Ranzato, Raia Hadsell, Maria-Florina Balcan, and Hsuan-Tien Lin (eds.), *Advances in Neural Information Processing Systems 33: Annual Conference on Neural Information Processing Systems 2020, NeurIPS 2020, December 6-12, 2020, virtual*, 2020. URL https://proceedings.neurips.cc/paper/2020/hash/1457c0d6bfcb4967418bfb8ac142f64a-Abstract.html.

Michael Chang, Sidhant Kaushik, Sergey Levine, and Tom Griffiths. Modularity in reinforcement learning via algorithmic independence in credit assignment. In Marina Meila and Tong Zhang (eds.), *Proceedings of the 38th International Conference on Machine Learning, ICML 2021, 18-24 July 2021, Virtual Event*, volume 139 of *Proceedings of Machine Learning Research*, pp. 1452–1462. PMLR, 2021. URL http://proceedings.mlr.press/v139/chang21b.html.

Lili Chen, Kevin Lu, Aravind Rajeswaran, Kimin Lee, Aditya Grover, Michael Laskin, Pieter Abbeel, Aravind Srinivas, and Igor Mordatch. Decision transformer: Reinforcement learning via sequence modeling. In A. Beygelzimer, Y. Dauphin, P. Liang, and J. Wortman Vaughan (eds.), *Advances in Neural Information Processing Systems*, 2021. URL https://openreview.net/forum?id=a7APmM4B9d.

J. Denavit and R. S. Hartenberg. A Kinematic Notation for Lower-Pair Mechanisms Based on Matrices. *Journal of Applied Mechanics*, 22(2):215–221, 06 1955. ISSN 0021-8936. doi: 10.1115/1.4011045. URL https://doi.org/10.1115/1.4011045.

Coline Devin, Abhishek Gupta, Trevor Darrell, Pieter Abbeel, and Sergey Levine. Learning modular neural network policies for multi-task and multi-robot transfer. In *2017 IEEE International Conference on Robotics and Automation, ICRA 2017, Singapore, Singapore, May 29 - June 3, 2017*, pp. 2169–2176. IEEE, 2017. doi: 10.1109/ICRA.2017.7989250. URL https://doi.org/10.1109/ICRA.2017.7989250.

Jacob Devlin, Ming-Wei Chang, Kenton Lee, and Kristina Toutanova. BERT: pre-training of deep bidirectional transformers for language understanding. In Jill Burstein, Christy Doran, and Thamar Solorio (eds.), *Proceedings of the 2019 Conference of the North American Chapter of the Association for Computational Linguistics: Human Language Technologies, NAACL-HLT 2019, Minneapolis, MN, USA, June 2-7, 2019, Volume 1 (Long and Short Papers)*, pp. 4171–4186. Association for Computational Linguistics, 2019. doi: 10.18653/v1/n19-1423. URL https://doi.org/10.18653/v1/n19-1423.

Benjamin Eysenbach, Abhishek Gupta, Julian Ibarz, and Sergey Levine. Diversity is all you need: Learning skills without a reward function. In *7th International Conference on Learning Representations, ICLR 2019, New Orleans, LA, USA, May 6-9, 2019*. OpenReview.net, 2019. URL https://openreview.net/forum?id=SJx63jRqFm.

Scott Fujimoto, Herke van Hoof, and David Meger. Addressing function approximation error in actor-critic methods. In Jennifer G. Dy and Andreas Krause (eds.), *Proceedings of the 35th International Conference on Machine Learning, ICML 2018, Stockholmsmässan, Stockholm, Sweden, July 10-15, 2018*, volume 80 of *Proceedings of Machine Learning Research*, pp. 1582–1591. PMLR, 2018. URL http://proceedings.mlr.press/v80/fujimoto18a.html.

M. Gori, G. Monfardini, and F. Scarselli. A new model for learning in graph domains. In *Proceedings. 2005 IEEE International Joint Conference on Neural Networks, 2005.*, volume 2, pp. 729–734 vol. 2, 2005. doi: 10.1109/IJCNN.2005.1555942.

Anirudh Goyal, Alex Lamb, Jordan Hoffmann, Shagun Sodhani, Sergey Levine, Yoshua Bengio, and Bernhard Schölkopf. Recurrent independent mechanisms. In *9th International Conference on Learning Representations, ICLR 2021, Virtual Event, Austria, May 3-7, 2021*. OpenReview.net, 2021. URL https://openreview.net/forum?id=mLcmdlEUxy-.

Danijar Hafner, Timothy P. Lillicrap, Jimmy Ba, and Mohammad Norouzi. Dream to control: Learning behaviors by latent imagination. In *8th International Conference on Learning Representations, ICLR 2020, Addis Ababa, Ethiopia, April 26-30, 2020*. OpenReview.net, 2020. URL https://openreview.net/forum?id=S1lOTC4tDS.

Wenlong Huang, Igor Mordatch, and Deepak Pathak. One policy to control them all: Shared modular policies for agent-agnostic control. In *Proceedings of the 37th International Conference on Machine Learning, ICML 2020, 13-18 July 2020, Virtual Event*, volume 119 of *Proceedings of Machine Learning Research*, pp. 4455–4464. PMLR, 2020. URL http://proceedings.mlr.press/v119/huang20d.html.

Donald J. Hejna III, Lerrel Pinto, and Pieter Abbeel. Hierarchically decoupled imitation for morphological transfer. In *Proceedings of the 37th International Conference on Machine Learning, ICML 2020, 13-18 July 2020, Virtual Event*, volume 119 of *Proceedings of Machine Learning Research*, pp. 4159–4171. PMLR, 2020. URL http://proceedings.mlr.press/v119/hejna20a.html.

Michael Janner, Qiyang Li, and Sergey Levine. Offline reinforcement learning as one big sequence modeling problem. In A. Beygelzimer, Y. Dauphin, P. Liang, and J. Wortman Vaughan (eds.), *Advances in Neural Information Processing Systems*, 2021. URL https://openreview.net/forum?id=wgeK563QgSw.

Yiding Jiang, Shixiang Gu, Kevin Murphy, and Chelsea Finn. Language as an abstraction for hierarchical deep reinforcement learning. In Hanna M. Wallach, Hugo Larochelle, Alina Beygelzimer, Florence d'Alché-Buc, Emily B. Fox, and Roman Garnett (eds.), *Advances in Neural Information Processing Systems 32: Annual Conference on Neural Information Processing Systems 2019, NeurIPS 2019, December 8-14, 2019, Vancouver, BC, Canada*, pp. 9414–9426, 2019. URL https://proceedings.neurips.cc/paper/2019/hash/0af787945872196b42c9f73ead2565c8-Abstract.html.

Vitaly Kurin, Maximilian Igl, Tim Rocktäschel, Wendelin Boehmer, and Shimon Whiteson. My body is a cage: the role of morphology in graph-based incompatible control. In *9th International Conference on Learning Representations, ICLR 2021, Virtual Event, Austria, May 3-7, 2021*. OpenReview.net, 2021. URL https://openreview.net/forum?id=N3zUDGN5lO.

Alexander Cong Li and Deepak Pathak. Functional regularization for reinforcement learning via learned fourier features. In A. Beygelzimer, Y. Dauphin, P. Liang, and J. Wortman Vaughan (eds.), *Advances in Neural Information Processing Systems*, 2021. URL https://openreview.net/forum?id=uTqvj8i3xv.

Tomás Mikolov, Kai Chen, Greg Corrado, and Jeffrey Dean. Efficient estimation of word representations in vector space. In Yoshua Bengio and Yann LeCun (eds.), *1st International Conference on Learning Representations, ICLR 2013, Scottsdale, Arizona, USA, May 2-4, 2013, Workshop Track Proceedings*, 2013. URL http://arxiv.org/abs/1301.3781.

Soroush Nasiriany, Vitchyr Pong, Steven Lin, and Sergey Levine. Planning with goal-conditioned policies. In Hanna M. Wallach, Hugo Larochelle, Alina Beygelzimer, Florence d'Alché-Buc, Emily B. Fox, and Roman Garnett (eds.), *Advances in Neural Information Processing Systems 32: Annual Conference on Neural Information Processing Systems 2019, NeurIPS 2019, December 8-14, 2019, Vancouver, BC, Canada*, pp. 14814–14825, 2019. URL https://proceedings.neurips.cc/paper/2019/hash/c8cc6e90ccbff44c9cee23611711cdc4-Abstract.html.

Emilio Parisotto, Lei Jimmy Ba, and Ruslan Salakhutdinov. Actor-mimic: Deep multitask and transfer reinforcement learning. In Yoshua Bengio and Yann LeCun (eds.), *4th International Conference on Learning Representations, ICLR 2016, San Juan, Puerto Rico, May 2-4, 2016, Conference Track Proceedings*, 2016. URL http://arxiv.org/abs/1511.06342.

Alec Radford, Jong Wook Kim, Chris Hallacy, Aditya Ramesh, Gabriel Goh, Sandhini Agarwal, Girish Sastry, Amanda Askell, Pamela Mishkin, Jack Clark, Gretchen Krueger, and Ilya Sutskever. Learning transferable visual models from natural language supervision. In Marina Meila and Tong Zhang (eds.), *Proceedings of the 38th International Conference on Machine Learning, ICML 2021, 18-24 July 2021, Virtual Event*, volume 139 of *Proceedings of Machine Learning Research*, pp. 8748–8763. PMLR, 2021. URL http://proceedings.mlr.press/v139/radford21a.html.

Kate Rakelly, Aurick Zhou, Chelsea Finn, Sergey Levine, and Deirdre Quillen. Efficient off-policy meta-reinforcement learning via probabilistic context variables. In Kamalika Chaudhuri and Ruslan Salakhutdinov (eds.), *Proceedings of the 36th International Conference on Machine Learning, ICML 2019, 9-15 June 2019, Long Beach, California, USA*, volume 97 of *Proceedings of Machine Learning Research*, pp. 5331–5340. PMLR, 2019. URL http://proceedings.mlr.press/v97/rakelly19a.html.

Alvaro Sanchez-Gonzalez, Nicolas Heess, Jost Tobias Springenberg, Josh Merel, Martin A. Riedmiller, Raia Hadsell, and Peter W. Battaglia. Graph networks as learnable physics engines for inference and control. In Jennifer G. Dy and Andreas Krause (eds.), *Proceedings of the 35th International Conference on Machine Learning, ICML 2018, Stockholmsmässan, Stockholm, Sweden, July 10-15, 2018*, volume 80 of *Proceedings of Machine Learning Research*, pp. 4467–4476. PMLR, 2018. URL http://proceedings.mlr.press/v80/sanchez-gonzalez18a.html.

F. Scarselli, Sweah Liang Yong, M. Gori, M. Hagenbuchner, Ah Chung Tsoi, and M. Maggini. Graph neural networks for ranking web pages. In *The 2005 IEEE/WIC/ACM International Conference on Web Intelligence (WI'05)*, pp. 666–672, 2005. doi: 10.1109/WI.2005.67.

Tom Schaul, Daniel Horgan, Karol Gregor, and David Silver. Universal value function approximators. In Francis Bach and David Blei (eds.), *Proceedings of the 32nd International Conference on Machine Learning*, volume 37 of *Proceedings of Machine Learning Research*, pp. 1312–1320, Lille, France, 07–09 Jul 2015. PMLR. URL https://proceedings.mlr.press/v37/schaul15.html.

Richard S. Sutton, Joseph Modayil, Michael Delp, Thomas Degris, Patrick M. Pilarski, Adam White, and Doina Precup. Horde: A scalable real-time architecture for learning knowledge from unsupervised sensorimotor interaction. In *The 10th International Conference on Autonomous Agents and Multiagent Systems - Volume 2*, AAMAS '11, pp. 761–768, Richland, SC, 2011. International Foundation for Autonomous Agents and Multiagent Systems. ISBN 0982657161.

Ian Tenney, Patrick Xia, Berlin Chen, Alex Wang, Adam Poliak, R Thomas McCoy, Najoung Kim, Benjamin Van Durme, Sam Bowman, Dipanjan Das, and Ellie Pavlick. What do you learn from context? probing for sentence structure in contextualized word representations. In *International Conference on Learning Representations*, 2019. URL https://openreview.net/forum?id=SJzSgnRcKX.

Emanuel Todorov, Tom Erez, and Yuval Tassa. Mujoco: A physics engine for model-based control. In *2012 IEEE/RSJ International Conference on Intelligent Robots and Systems, IROS 2012, Vilamoura, Algarve, Portugal, October 7-12, 2012*, pp. 5026–5033. IEEE, 2012. doi: 10.1109/IROS.2012.6386109. URL https://doi.org/10.1109/IROS.2012.6386109.

Ashish Vaswani, Noam Shazeer, Niki Parmar, Jakob Uszkoreit, Llion Jones, Aidan N. Gomez, Lukasz Kaiser, and Illia Polosukhin. Attention is all you need. In Isabelle Guyon, Ulrike von Luxburg, Samy Bengio, Hanna M. Wallach, Rob Fergus, S. V. N. Vishwanathan, and Roman Garnett (eds.), *Advances in Neural Information Processing Systems 30: Annual Conference on Neural Information Processing Systems 2017, December 4-9, 2017, Long Beach, CA, USA*, pp. 5998–6008, 2017. URL https://proceedings.neurips.cc/paper/2017/hash/3f5ee243547dee91fbd053c1c4a845aa-Abstract.html.

Jesse Vig and Yonatan Belinkov. Analyzing the structure of attention in a transformer language model. In Tal Linzen, Grzegorz Chrupala, Yonatan Belinkov, and Dieuwke Hupkes (eds.), *Proceedings of the 2019 ACL Workshop BlackboxNLP: Analyzing and Interpreting Neural Networks for NLP, BlackboxNLP@ACL 2019, Florence, Italy, August 1, 2019*, pp. 63–76. Association for Computational Linguistics, 2019. doi: 10.18653/v1/W19-4808. URL https://doi.org/10.18653/v1/W19-4808.

Nelson Vithayathil Varghese and Qusay H. Mahmoud. A survey of multi-task deep reinforcement learning. *Electronics*, 9(9), 2020. ISSN 2079-9292. doi: 10.3390/electronics9091363. URL https://www.mdpi.com/2079-9292/9/9/1363.

Tingwu Wang, Renjie Liao, Jimmy Ba, and Sanja Fidler. Nervenet: Learning structured policy with graph neural networks. In *6th International Conference on Learning Representations, ICLR 2018, Vancouver, BC, Canada, April 30 - May 3, 2018, Conference Track Proceedings*. OpenReview.net, 2018. URL https://openreview.net/forum?id=S1sqHMZCb.

A Policy Optimization

We choose to employ TD3 Fujimoto et al. (2018) for optimizing our policy because it is highly efficient and consistently performs well for MuJoCo-like Todorov et al. (2012) agents. Efficiency is an important consideration in agent-agnostic reinforcement learning because training with up to 32 morphologies can require large amounts of experience otherwise. Following the TD3 algorithm, we sample exploratory actions from a normal distribution $\mathcal{N}(\mathbf{a}_t, \sigma^2)$ where $\mathbf{a}_t$ is the mean action, and the variance σ^2 is a hyperparameter that controls the degree of randomness in the exploration policy of TD3. Following prior work Huang et al. (2020) we store a separate replay buffer of transitions for each training morphology, and alternate between collecting environment steps and training for each morphology in lockstep. We train each agent for up to 3 million environments steps total across all training morphologies, and run 4 random seeds per method. Our model fits on a single Nvidia 2080ti GPU, and requires seven days of training to reach 3 million environments steps. We provide a table of hyperparameters in Appendix B for our policy and reinforcement learning optimizer.

B Hyperparameters

In this section, we describe the hyperparameters used with our model. These include hyperparameters in our model architecture, as well as hyperparameters for the TD3 optimizer that we use to optimize our policy. The hyperparameters for our model architecture can be found in the below table, while hyperparameters for TD3 can be found two tables below.

Hyperparameter Name	**Hyperparameter Value**
D (Token Embedding Size)	32
M (Sinusoidal Embedding Size)	96
Transformer Hidden Size	128
Transformer Feedforward Size	256
Attention Heads	2
Transformer Encoder Layers	3
Transformer Decoder Layers	3
Transformer Activation	relu
Dropout Rate	0.0

Table 2: Hyperparameters for our model architecture.

In the below table, we report the standard hyperparameters that are typically exposed to the user in TD3. Note that we employ the same TD3 hyperparameters across every task, which demonstrates our model does not require per-task tuning.

Hyperparameter Name	**Hyperparameter Value**
Num Random Seeds	4
Batch Size	100
Max Episode Length	1000
Max Replay Size Total	10000000
Max Environment Steps	3000000
Policy Update Interval	2
Initial Exploration Steps	10000
Policy Noise	0.2
Policy Noise Clip	0.5
τ	0.046
σ	0.126
Discount Factor	0.99
Gradient Clipping	0.1
Learning Rate	0.00005

Table 3: Hyperparameters for our TD3 implementation.

We use identical hyperparameters for the Amorpheus Kurin et al. (2021) and Shared Modular Policies Huang et al. (2020) baselines, except we update the learning rate to 0.0001, which we found to result in the best performance for both methods. We use the same reinforcement learning framework as Kurin et al. (2021) and Huang et al. (2020) for our experiments.

C HELD OUT MORPHOLOGIES

In this section, we present a table that shows which morphologies are used for training and which morphologies are used for testing for each kind of agent. For tasks that mix multiple kinds of agents, the training morphologies for each kind are mixed, and the testing morphologies are mixed, but no training morphology becomes a testing morphology and vice versa.

Task	**Training Morphologies**	**Testing Morphologies**
Cheetahs		
	cheetah_2_back	cheetah_3_balanced
	cheetah_2_front	cheetah_5_back
	cheetah_3_back	cheetah_6_front
	cheetah_3_front	
	cheetah_4_allback	
	cheetah_4_allfront	
	cheetah_4_back	
	cheetah_4_front	
	cheetah_5_balanced	
	cheetah_5_front	
	cheetah_6_back	
	cheetah_7_full	
Walkers		
	walker_2_main	walker_3_main
	walker_4_main	walker_6_main
	walker_5_main	
	walker_7_main	
Humanoids		
	humanoid_2d_7_left_arm	humanoid_2d_7_left_leg
	humanoid_2d_7_lower_arms	humanoid_2d_8_right_knee
	humanoid_2d_7_right arm	
	humanoid_2d_7_right leg	
	humanoid_2d_8_left knee	
	humanoid_2d_9_full	
Hoppers		
	hopper_3	
	hopper_4	
	hopper_5	

Table 4: Morphologies used for training and testing.

D DETAILS OF ROBUSTNESS EXPERIMENT

In the main paper, we performed an experiment testing the robustness of our approach versus Amorpheus Kurin et al. (2021) and Shared Modular Policies Huang et al. (2020) baselines. In order to determine the order in which sensors "break," simulated by replacing sensor readings with random noise sampled from the standard normal distribution, we visualized the cross attention weights in the final decoder layer of our Transformer policy, and sorted the sensors in increasing order according to how frequently our policy attends to them throughout an episode. Specifically, we take the average value of the final cross attention mask throughout an episode, and average again over the queries axis, in order to obtain a vector with $N_S(n)$ elements, representing the average attention weight applied to

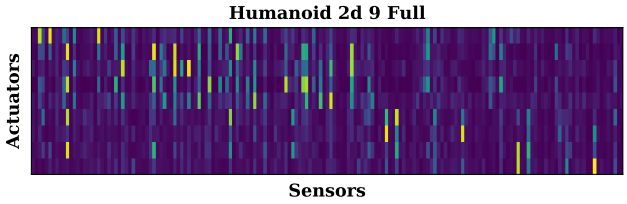

Figure 6: Visualization of the cross attention weights in the final layer of our policy model on the Humanoids task and Humanoid 2d 9 Full morphology. Each cell in the attention matrix corresponds to the maximum attention value for that cell over an entire episode. Cells with dark shading indicate that our model ignores those sensors over an entire episode by zeroing their attention weights.

a given sensor by *any* actuator through an episode. In order to corrupt a particular fraction c of the agent's sensors, we replace the first $\lceil c \cdot N_S(n) \rceil$ sensors with random noise, according to their sorted order as previously described. This methodology ensures that sensor corruptions are cumulative. That is, for two given fractions $c_1 > c_0$, the sensors corrupted by c_0 are also corrupted by c_1.